OPEN ACCESS
IOP Publishing | International Atomic Energy Agency Nuclear Fusion
Nucl. Fusion **63** (2023) 096010 (19pp) https://doi.org/10.1088/1741-4326/ace2d2

Fuel desorption from JET-ILW materials: assessment of analytical approach and identification of sources of uncertainty and discrepancy

Y. Zayachuk[1,*], I. Jepu[1,2], M. Zlobinski[3], C. Porosnicu[2], N. Catarino[4], E. Pajuste[5], P. Petersson[6], L. Dittrich[6], J.P. Coad[1], E. Grigore[2], C. Postolache[7], E. Alves[4], G. Kizane[5], M. Rubel[6] and A. Widdowson[1]

[1] United Kingdom Atomic Energy Authority, Culham Centre for Fusion Energy, Culham Science Centre, Abingdon, OXON OX14 3DB, United Kingdom of Great Britain and Northern Ireland
[2] National Institute for Laser, Plasma and Radiation Physics, Măgurele 077125, Romania
[3] Forschungszentrum Jülich GmbH, Institut für Energie- und Klimaforschung—Plasmaphysik, Partner of the Trilateral Euregio Cluster(TEC), 52425 Jülich, Germany
[4] IPFN, Instituto Superior Técnico, Universidade de Lisboa, 1049-001 Lisboa, Portugal
[5] University of Latvia, Institute of Chemical Physics, Riga LV-1004, Latvia
[6] KTH Royal Institute of Technology, Fusion Plasma Physics, 100 44 Stockholm, Sweden
[7] National Institute for Physics and Nuclear Engineering, 'Horia Hulubei' IFIN HH, Măgurele 077125, Romania

E-mail: yevhen.zayachuk@ukaea.uk

Received 19 October 2022, revised 25 April 2023
Accepted for publication 29 June 2023
Published 31 July 2023

Abstract

This work was carried out to identify sources of errors, uncertainties and discrepancies in studies of fuel retention in wall components from the JET tokamak using methods based on thermal desorption. Parallel aims were to establish good practices in measurements and to unify procedures in data handling. A comprehensive program designed for deuterium quantification comprised the definition and preparation of two types of materials (samples of JET limiter Be tiles and deuterium-containing targets produced in the laboratory by magnetron-assisted deposition), their pre-characterization, quantitative analyses of the desorption products in three different thermal desorption spectroscopy systems and a detailed critical comparison of the results. Tritium levels were also determined by several techniques in samples from JET and in tritiated targets manufactured specifically for this research program. Facilities available for studies of Be- and tritium-contaminated materials from JET are presented. Apparatus development, future research options and challenges are discussed.

Keywords: fuel retention, thermal desorption, dissolution, JET-ILW

(Some figures may appear in colour only in the online journal)

* Author to whom any correspondence should be addressed.

List of Acronyms

Acronym	Meaning
AIMS	Accelerator-based *in situ* material surveillance
AMS	Accelerator mass spectroscopy
ASDEX	Axially Symmetric Divertor Experiment
BIXS	Beta-induced x-ray spectroscopy
CCFE	Culham Centre for Fusion Energy, Culham, United Kingdom
D	Deuterium (^{2}H)
ERDA	Elastic recoil detection analysis
FTS	Fast transfer system
FZJ	Forschungszentrum Jülich, Jülich, Germany
GDOES	Glow discharge optical emission spectroscopy
HIERDA	Heavy ion elastic recoil detection analysis
HiPIMS	High power impulse magnetron sputtering
IAP	Institute of Atomic Physics, Magurele, Romania
IBA	Ion beam analysis
ILW	ITER-like wall
IPT	Imaging plate technique (radiography)
IST	Instituto Superior Tecnico, Lisbon, Portugal
IWGL	Inner wall guard limiter
JET	Joint European Torus
JET-C	JET with carbon wall
JET-ILW	JET with ITER-like wall
KTH	Kungliga Tekniska Högskolan Royal Institute of Technology, Sweden
LEIS	Low-energy ion scattering
LIAS	Laser-induced ablation spectroscopy
LIBS	Laser-induced breakdown spectroscopy
LID(S)	Laser-induced desorption (spectroscopy)
LSC	Liquid scintillography counter
MS	Magnetron sputtering
NRA	Nuclear reaction analysis
QMS	Quadrupole mass spectroscopy
RBS	Rutherford backscattering spectrometry
PFC	Plasma-facing components
PFM	Plasma-facing materials
PFS	Plasma-facing surface
RH	Remote handling
SIMS	Secondary ion mass spectroscopy
T	Tritium (^{3}H)
TEXTOR	Tokamak Experiment for Technology Oriented Research
TFTR	Tokamak Fusion Test Reactor
TDS	Thermal desorption spectroscopy
ToF-ERDA	Time-of-flight ERDA
UoL	University of Latvia
UU	Uppsala University, Sweden
WPL	Wide poloidal limiter

1. Introduction

Fuel retention studies in controlled fusion devices provide a basis for the assessment of fuel balance and the tritium (T) inventory in current machines and for predictions of the inventory resulting from deuterium–tritium (D–T) operation in future reactors [1–3]. Regular determination of gas balance and D content in PFCs was carried out in the past in ASDEX Upgrade [4, 5], TEXTOR [6–8], TFTR [9, 10] and JET [11–15] tokamaks. The full extent of the issues posed by T accumulation was realized after TFTR [9, 10] and JET [13–17] operations with a 1:1 D–T mixture, namely long-term in-vessel retention reaching 35% of the gas input [14]. This, in turn, accelerated both retention studies and work towards the development of fuel control and removal methods [2]. The latter did not bring promising results in carbon-wall devices [18]. The breakthrough in the reduction of fuel retention came with the major change of wall materials in JET, namely the transition from JET-C to JET-ILW with W in the divertor and Be on the main chamber wall [19, 20]. This strong reduction in the carbon source led to the decrease of fuel retention by a factor of 10–20 in comparison with the situation in JET-C [21–23].

Fuel measurements in PFCs fall into two major categories summarized in table 1: without breaking vacuum (in the following called '*in situ*') and after venting the torus and retrieval of wall components for analysis in the lab ('*ex situ*'). Studies inside the vented machine during shutdowns will not be addressed here. This approach is not practiced in JET at present because it would require analytical systems integrated with the RH equipment for operations in Be- and T-contaminated environments.

The category of *in situ* methods comprises optical spectroscopy [24, 25] and gas-balance assessment [7, 26–28], while T accounting in D–T operation is also based on radiometric, chromatographic and calorimetric measurements [29, 30]. This category may be complemented by LIDS, LIBS or LIAS spectroscopy techniques [31–36], but to date a rather limited number of *in situ* measurements of local character have been performed, including one experiment in JET-C [31]. *Ex situ* analyses are carried out using a large number of tools employing various means for fuel thermal release, a range of IBA techniques and a set of methods for determination of T content. Their major features, advantages and drawbacks are summarized in table 1. Many of these methods have been used for fuel studies in JET materials. However, some of the existing techniques, for example *in situ* IBA [37], cannot be applied at JET because of the machine's size and radioactive environment.

Despite broad research programs and a range of analytical tools used in retention studies, at least two issues in the assessment of retention remain unresolved. These are the discrepancies between: (i) the global gas balance and the assessment based on results of post-exposure measurements on PFCs retrieved from tokamaks where a difference of a factor of up to two was reported on several occasions [7, 26–28]; (ii) results obtained by TDS in different laboratories when analyzing apparently the same type of wall material (e.g. wall tiles) retrieved from a given tokamak.

The reported differences of a factor of up to two between the D balance and *ex situ* analyses [7, 26–28] may be attributed to (i) an immediate release and/or H–D isotope exchange upon PFC exposure to the ambient atmosphere and (ii) inaccuracy in the extrapolation of local surface measurements to the whole machine. Fast processes of D release or H–D isotope exchange

Table 1. Analysis of hydrogen isotopes in controlled fusion devices with emphasis on JET (list limited to methods used in fuel retention studies).

Category	Technique	Advantages	Disadvantages/limitations	Remarks/references
In situ	Optical spectroscopy	H/D ratio		[25, 29]
	Gas input/feed	Direct measurement of gas flow and pressure		Essential to prepare and sustain discharges
	Gas balance by QMS	Direct measurements: shot-by-shot or after operation day		Common in most machines [7, 26–28]
	Radiometry: beta and gamma	(a) Assessment of T from D–D reaction. (b) Activation by DD and DT neutrons	Low accuracy. Limited to PFC surface in areas accessible by RH	Possible only during shut-down period
	AIMS	Inter-shot study	Limited to small and medium-size machines without permanent magnetic field	Only early tests performed in Alcator C-Mod [37]
	Calorimetry	Precise determination of T inventory in the storage bed		[29, 30]
	LIAS	Spatial analysis		JET [31], TEXTOR [32, 33, 38]
	LIDQMS	Spatial analysis. Inter-shot analysis		TEXTOR [32]. Under development for ITER Test in JET under preparation
	LIBS	Spatial analysis		Tested in laboratory. Limited *in situ* experiments on JET [39, 40]. Proposal for RH system for deployment during in-vessel maintenance
Ex situ	TDS—flash/fast temperature ramp	Fast qualitative assessment of H isotopes in PFC	Need for cross-calibration	Process occurs also *in-situ* from PFC under high heat load/transient events. Flash lamp tested on JET tiles for fuel removal, but the isotope release was not directly monitored [41]
	TDS—steady temperature ramp	Determination of binding states. Total inventory if combined with outgassing at maximum temperature	Need for calibration using calibrated leak. Temperature limited to 1273 K in most systems	Temperature limited to 1073 K for Be samples (evaporation) [42]
	NRA for H $p(^{15}N,\alpha)^{12}C$	Selective for H	Expensive ^{15}N. Information depth limited <1 μm	Not done on JET materials
	NRA for D $D(^{3}He,\alpha)^{4}He$	Quantification and depth profiling down to 20 μm in low-Z substrates	Expensive ^{3}He. Overlap of C and Be peaks make low concentrations hard to deconvolve	Most important and always used method for PFC analysis [43–55]. Simultaneous analysis of C, Be but the information depth is too small for thick co-deposits even with a 6 MeV beam [56]
	NRA for T $T(^{12}C,\alpha)^{11}B$ $T(^{12}C,p)^{14}C$ $T(d,\alpha)n$		Low sensitivity of ^{12}C-t reactions. Neutron generation in d-t reaction.	Both ^{12}C–t reactions tried on JET materials [57], while the d–t reaction was used on TFTR tiles [58]

(Continued.)

Table 1. (Continued.)

Category	Technique	Advantages	Disadvantages/limitations	Remarks/references
	ERDA	Quantitative depth profiling of all isotopes	Information depth <1 μm	[43, 59–61]
	AMS	Depth profiling of all H isotopes	Difficult sample preparation	[62]
	GDOES	Detection and depth profiling of all H isotopes. Large information (sputter) depth possible up to 100 μm	Problems with calibration for D	[63]
	SIMS	Detection and depth profiling of all H isotopes and He. Isotopic ratio at a given depth. Large information (sputter) depth possible	Challenging quantification in mixed materials. Sensitivity depends on chemical surrounding/material composition	[15, 42, 64]
	LIAS			Under development. Not tested in vessel during JET shutdow
	LIDS and LID-QMS	Rapid desorption	Need for calibration using calibrated leak. Risk of desorption from the spot-adjacent region	[65]
	LIBS			[66, 67]
Ex situ for T	Off-gassing			T analysis: isotopic exchange of released T in water vapor. Dissolution of HTO in water bubbler and analysis by LSC
	Radiography (IPT)	T distribution map in the surface and subsurface layer up to 4 μm dependent on the substrate and co-deposit composition. In combination EPMA/ EDX T determination in individual elements	Limited and substrate dependent information depth. No quantification	[68–72]
	BIXS	T distribution map in the surface and subsurface layer up to 4 μm dependent on the substrate and co-deposit composition. Information on other species based on x-ray spectrum		[73]
	TDS		QMS systems have relatively high limit of detection level compared with radiometric detection methods	T analysis by LSC [74]. T analysis by proportional counter [75]. T analysis by QMS discussed in this work.
	Full combustion			T analysis by LSC [74]
	Dissolution			T analysis by LSC [76]

are difficult to study using wall probes because the shortest interval between the probe exposure and D analysis amounts to several hours, i.e. the time necessary for probe withdrawal, venting of the probe system, retrieval of material and transfer to the surface analysis station. The D content measured after such 'transfer' time is fairly stable: the decrease of the retained D is up to 25% over 5 years from that initially determined value [77]. It should be stressed that such measurements are

possible only in medium sized machines, such as TEXTOR [77], operated with relatively easy access to the probe systems. No studies of that kind have been performed in JET, although a FTS for surface probes was originally constructed [78]. This facilitated the transfer in vacuum of the exposed probe from the torus to a surface analysis station, but the operation was complex and the system was used on only a very few occasions [6, 79] and due to conflicting changes to the furniture within the JET vessel was dismantled in the early 1990s. In practice, the time between the end of plasma operation in JET (start of shutdown) and surface measurements is at least 3–4 months. Secondly, the global balance data are based on daily or long-term fuel accountancy (injected versus pumped-out amount) in the whole machine, while surface analyses can be carried out only for a limited number of wall tiles available for retrieval and *ex situ* studies. Even the best planned tile selection does not provide full poloidal and toroidal coverage. This in turn may lead to inaccurate assessment of total inventory, because the extrapolation is done under the assumption of toroidal symmetry of the erosion–deposition patterns.

The second category of discrepancies or difficulties in TDS studies arises from significant local variations of fuel retention in the PFCs, in extreme cases also on a micro-scale because of the imperfections in surface topography or tile alignment [59, 80, 81]. As a consequence, TDS from adjacent areas, even located only a few millimeters apart and of apparently identical appearance, often yields very different results, and the repetition of destructive TDS measurements on the same sample but under different conditions or in another laboratory is of course impossible. The approach based on a comparison between results of IBA and TDS may be reliable if a very detailed pre-characterization of materials by IBA is performed beforehand. All such aspects are taken into account in the work presented below.

This work focuses on a comparison and critical assessment of thermal desorption data obtained at various laboratories studying JET samples and lab-produced reference samples manufactured specifically for this research program. The overall aim is to improve quantification and further develop good practices in the characterization of PFC in order to improve reliability (consistency) in predictions of fuel inventory in a reactor-class machine such as ITER. For that reason, and in the view of the ongoing D–T operation in JET [82], methods for T analysis are also discussed, although the quantities of that isotope in JET-ILW materials from the three initial ILW campaigns are at a low level, not exceeding 1 MBq (or $\sim 5.5 \times 10^{14}$ T atoms) per analyzed sample of 0.1–0.3 cm^3.

This paper provides an overview of experimental procedures and possible sources of errors and/or discrepancies. The experimental approach is presented, describing selection, preparation and pre-characterization of JET materials and laboratory-produced reference samples. The analytical capabilities of several laboratories participating in this study are presented. A comprehensive section with results for D and T retention is concluded with recommendations regarding procedures in analysis and selection of reference materials.

2. Experiment

The pre-requisite for comparative studies of D and T retention is the availability of specimens with contents of the species to be quantified upon thermal release as close to each other as possible. Several types of samples of this kind were selected and manufactured: (a) pieces of the castellated bulk Be limiters (retrieved from JET); (b) Mo plates coated with a magnetron-deposited layer of W co-deposited with either H or D (lab produced); (c) Mo plates coated with a layer of T-saturated W (lab produced). Measurements included TDS, IBA and the dissolution method (only for T). Details are given in the following sub-sections.

2.1. Samples retrieved from JET—beryllium limiters

Fuel retention in all types of PFCs retrieved from JET has been examined with IBA and TDS in the past [42–55, 83].

Based on the obtained knowledge about the erosion–deposition and fuel retention patterns, decisions were made regarding sample selection and preparation. Samples used for detailed study were produced from the Be tiles of an outer WPL (tile 4D14) and an IWGL (tile 2XR10) retrieved during the shutdown following the third ILW campaign [50]. Some additional samples from the upper dump plate (tile 2B2C), retrieved after the same campaign, were also used. Figure 1 shows the images of the selected tiles and their corresponding locations within the poloidal cross-section of the JET vessel.

Individual 12 mm × 12 mm × 12 mm castellations were cut from several positions across the tiles (marked by crosses and identification numbers in figure 1); these positions cover the entire toroidal width of a tile, and thus the selected castellations capture erosion and deposition zones, representing different mechanisms of fuel retention. An optimized cutting procedure was used, implementing an extra-hard, carbide-type band saw capable of processing beryllium material in dry conditions (i.e. no water is involved in the process). The sample temperature during the cutting process did not exceed 55 °C, to avoid release of D and T during the cutting, and was continuously measured using an infrared camera. Then, each castellation was further cut into a set of four so-called 'quarter samples' (sized 5.5 mm × 5.5 mm × 1.5 mm), labeled A to D. All cutting was done at the IAP, Romania, using procedures described in [53]. The D content in the surface layers of the respective pieces was then determined by means of IBA (NRA and RBS), using a 2.5 MeV $^3He^+$ beam at the IST, Portugal. Following this, samples were distributed to four participating laboratories: (1) IAP (referred to in the following discussion as Facility A), (2) CCFE (Facility B), (3) (UoL; Facility C) and (4) (FZJ; Facility D), for TDS (IAP, CCFE and FZJ) and dissolution (UoL) measurements.

2.2. Laboratory-produced samples—tungsten-coated molybdenum

These samples, referred to as the 'reference samples', were produced at IAP using HiPIMS. A nominally 2 μm thick W

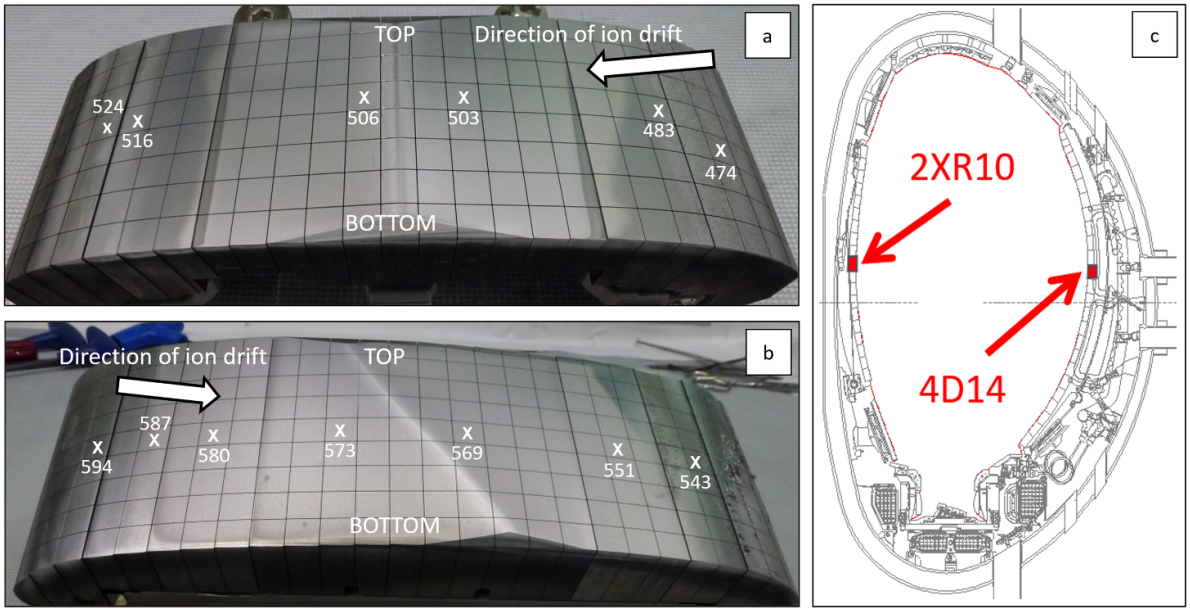

Figure 1. Images of Be tiles where quarter samples were cut, with crosses indicating individual castellations that were used for producing them: (*a*) IWGL tile 2XR10; (*b*) WPL tile 4D14; (*c*) poloidal locations of these tiles.

layer with D was deposited on a polished Mo substrate with dimensions of 12 mm × 12 mm × 1 mm. All samples were manufactured in a single run to maximize sample uniformity. Two samples were sent to each of the three participating laboratories (IAP, CCFE and FZJ) for TDS measurements; these were performed on the same day in each participating lab to ensure that the discrepancy in measured contents due to a difference in time delay between manufacturing and measurement was eliminated. In parallel, two other sets of samples were analyzed by ion beam methods to determine the gas content and sample purity (see section 2.5).

2.3. Laboratory-produced samples—tritiated tungsten-coated molybdenum

Laboratory-produced tritiated W-coated Mo samples are referred to as 'tritiated samples'. A set of samples with 2 μm W coated on a Mo plate, obtained as described in the previous section but not having any gas inclusions, were placed in a Pyrex glass tube using spacers consisting of glass rings 10 mm in diameter and 5 mm thick and quartz wool (see figure 2(*a*)). The glass ampoule with W-coated Mo samples was placed inside a tubular furnace (RT 50–250/11) with a Nabertherm-type temperature controller and connected at a T manifold with a vacuum facility (see figure 2(*b*)).

The glass ampoule with W–Mo samples was first evacuated at room temperature (1 h at a pressure below 1 Pa) and degassed at 1273 K (1 h at a pressure below 1.3 × 10^{-2} Pa). The W–Mo samples were put in contact with a T_2:^{3}He mixture extracted from an old T gas source [84]. The samples were kept in the T_2:^{3}He atmosphere for 196 h at 200 °C, followed by slow decrease of the temperature to room temperature, then maintained at this temperature for a minimum

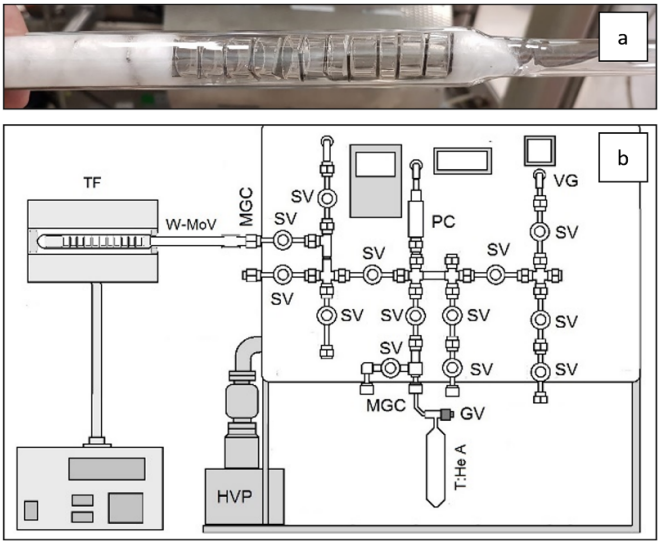

Figure 2. (*a*) The glass vials with W–Mo samples and (*b*) facility for tritiation of W–Mo samples (TF, tubular furnace, glass vials with W–Mo samples; MGC, metal–glass connectors; HVP, high-vacuum pump; SV, Swagelok valves; GV, glass valves; PC, pressure controller; VG, vacuum gauge; T:He A, T_2:^{3}He ampoule).

of 8 h. The residual T_2:^{3}He was transferred to the glass ampoule using a Toepler pump and the T trace removed using a HVP.

The activity of the tritiated W–Mo samples was determined by a total combustion method [85]. Two samples were analyzed using a total combustion/calcination facility. The total combustion/calcination facility consisted of (a) an oxygen supply, (b) a tandem tubular furnace, first for combustion/calcination of samples and secondarily for catalytic oxidation

of the flue gases, and (c) a collector for tritiated water using the bubbling principle, with four retention vials. The total combustion protocol was as follows:

- oven/CuO catalytic bed temperature: 800 °C
- oven/sample incineration temperature: 1000 °C
- oxygen flow rate: 4 l min^{-1}
- combustion boat made of Cu
- added to the the combustion boat: 2 g of anhydrous natrium carbonate for retention of molybdic anhydride vapors generated in the calcination step
- HTO retention: fresh distillate water (four vials with 5 ml each)
- HTO activity from the retention vial determination by 1 ml sampling in a 16 ml ULTIMA- GOLD M liquid scintillator and activity measured with a LSC (TRICARB TR2800 Perkin Elmer)
- determination of oxidation and HTO retention yield using a sample contaminated with testosterone-1,2-T in a controlled way. The obtained value was 94% ± 3% [86].

The mean activity on the two samples was determined to be 160 ± 2.895 MBq.

2.4. Thermal desorption measurements

TDS measurements were performed at three participating laboratories. Samples measured in each have the corresponding index, for example 463A for a sample measured at Facility A.

- IAP (Facility A; [87]): the heating system of this instrument is an oven, with samples being placed in the quartz tube; it provides a programmable heating rate up to 15 K min^{-1}, with a maximum temperature of 1323 K. Temperature control is provided by a type K thermocouple placed inside the oven; the actual temperature on the sample is deduced based on calibration (sample temperature as a function of oven temperature). Gas analysis is performed with a QMS located around a 90° corner at ∼50 cm from the sample. Be- and T-containing samples can be analyzed.
- CCFE (Facility B; [88]): the heating system is a Mo heating plate, with samples placed on it; it has a heating rate up to 30 K s^{-1}, with a maximum temperature of 1273 K. Temperature control is provided by a type K thermocouple attached to the heater such that the temperature of the heater is measured and recorded; sample temperature is assumed to be equal to that of the heater. Gas analysis is performed with a line-of-sight QMS, with the distance between the sample surface in the measurement position and QMS head ∼24 mm; the QMS is not differentially pumped. Be- and T-containing samples can be analyzed. Special measures are taken when Be samples are measured: (1) the maximum temperature is limited to 1050 K because Be evaporation occurs at higher temperatures (which is undesirable and needs to be avoided because it leads to contamination of the detector, vacuum chamber and its windows); (2) a protective layer of AlN is placed between the sample and heater to avoid adhesion of the sample to the heater at elevated temperature.
- FZJ (Facility D; [89]): the heating system of this instrument is an oven, with samples being placed in the quartz tube, similarly to Facility A. Heating rates of up to 100 K min^{-1} are possible, with a maximum temperature of 1433 K. Gas analysis is performed with two QMSs simultaneously, capable of discriminating D_2 and He, located around a 90° corner at ∼80–95 cm from the sample, respectively. The temperature for the heating control is measured with a type K thermocouple inside the quartz tube. The temperature of the thermocouple is equal to that of the sample because of the homogeneous heating from all sides, the small size of the sample and the slow heating rate, so that the system is always in thermal equilibrium. Be- and T-containing samples can be analyzed. Be samples are covered by a smaller, exchangeable quartz half-tube that provides a large exit for the desorbed gases through a quartz labyrinth that hinders evaporating Be from contaminating the main quartz tube.

To unify the conditions of thermal treatment so as to make inter-laboratory comparisons possible, identical heating scenarios were applied in all participating TDS facilities for the quarter and reference samples, as follows:

- Quarter samples—heating rate 10 K min^{-1}, maximum temperature 1050 K, hold time at maximum temperature 1 h. Signals of masses 3 (HD molecules), 4 (D_2 and HT), 5 (DT) and 6 (T_2) were monitored to quantify the amounts of D and T released. Atomic D release flux F_D was calculated as a sum

$$F_D = F_{HD} + 2F_{D2} \quad (1)$$

  where F_{HD} and F_{D2} are molecular release fluxes of masses 3 and 4, respectively. Atomic T release flux F_T was calculated as a sum

$$F_T = F_{DT} + 2F_{T2} \quad (2)$$

  where F_{DT} and F_{T2} are the molecular release fluxes of masses 5 and 6, respectively. In addition, signals of masses 18 (H_2O) and 20 (D_2O and HTO) were recorded.
- Reference samples—heating rate 10 K min^{-1}, maximum temperature 1275 K, hold time at maximum temperature 1 h. Signals of masses 3 and 4 (HD and D_2) were monitored to quantify released amounts of D, using equation (2). In addition, signals of masses 18 (H_2O), 19 (HDO) and 20 (D_2O and HTO) were recorded.
- Tritiated sample—heating rate 10 K min^{-1}, maximum temperature 1275 K, hold time at maximum temperature 1 h. Signals of masses 4 (HT molecules) and 6 (T_2) were monitored to quantify released amounts of T. Atomic T release flux F_T in the case of these samples was calculated as

$$F_T = F_{HT} + 2F_{T2} \quad (3)$$

where F_{HT} and F_{T2} are molecular release fluxes of masses 4 and 6, respectively. In addition, signals of masses 18 (H_2O), 19 (HDO), 20 (D_2O and HTO), 21 (DTO) and 22 (T_2O) were recorded.

In all facilities, quantification of measured release signals was performed using calibrated leaks. A H_2 calibrated leak was used for determination of the calibration factor for the mass 2 release signal, a D_2 calibrated leak was used for the calibration factor for the mass 4 release signal in the case of D-containing samples, a He leak was used for the calibration factor for the mass 4 release signal in the case of He-containing samples. The mass 3 calibration factor (HD molecules) was calculated as an average of the factors for masses 3 (H_2) and 4 (D_2). Factors for masses 5 and 6 (DT and T_2 molecules) were calculated by linear extrapolation of factors for masses 2 (H_2) and 4 (D_2). Other signals were not quantified.

2.5. IBA measurements

IBA was performed at IST and at the UU, Sweden.

At IST, retention of D was measured using the 2.5 MV van de Graaff accelerator at the Laboratory of Accelerators and Radiation Technologies [90]. The accelerator is equipped with a chamber dedicated to fusion research, where Be- and T-containing samples are handled. RBS and NRA were performed using ^{3}He ions at an energy of 2.3 MeV, in order to measure the amounts of D in the investigated Be samples; NRA of W and Be samples was based on proton and alpha-particle detection from D(^{3}He,p)^{4}He. All quarter Be samples were measured before TDS analysis and a selection measured after TDS.

At UU, measurements were performed at the Tandem Laboratory located at the Ångström Laboratory of UU. The laboratory has capabilities for handling radioactive and contaminated materials. A 5 MeV National Electrostatics Pelletron was used to examine W-coated samples by time-of-flight (ToF) HIERDA in a gas ionization chamber [60] using a 36 MeV $^{127}I^{8+}$ beam and NRA with a 4.5 MeV $^3He^+$ beam. ToF-HIERDA allowed for a detailed quantitative determination of surface composition and depth profiling of H to W (up to a depth of 2000 $\times$ 10^{15} atoms cm^{-2}, which approximately corresponds to $\sim$320 nm assuming a standard W density of 19.25 g cm^{-3}), while the total amount of D in the W-coated samples was determined by NRA.

2.6. Dissolution tritium measurements

Dissolution measurements were performed at the UoL (Facility C). Details of the experimental setup can be found in [91]. In this technique, investigated samples are etched chemically (Be samples, using sulfuric acid) or electrochemically (W samples, using 30% KOH solution) such that T is released simultaneously with the dissolution of the sample. T is released in molecular and atomic forms as part of different chemical compounds in liquid and gas phases. The amount of T is determined radiometrically, with the activity measured in the liquid phase by LSC and in the gas phase by a proportional counter and T monitor (TEM 2102 A, Mab Solutions GmbH).

3. Results

3.1. Quarter samples

Quarter samples were first characterized using IBA. Figure 3 presents comparison of D retention values obtained by IBA of quarter samples, superimposed with IBA data taken across the whole tile prior to cutting. Measurements on quarter samples compare well with the results of whole-tile scans, capturing the distribution of D across the tile as well as actual values of D retention. At the same time, they demonstrate that there is a difference in measured D content between quarters within the same set, even though they originate from the same castellation. The difference in D retention between the individual quarters (within a set) ranges between factors of 1.3 and 2.4, with the factor of difference averaged over all sample sets being $\sim$1.5 (or 50%).

Comparison of the total D retention for TDS measurements at different facilities, plotted as a function of position within the tile of origin, is presented in figure 4. It can be seen that the values of retention obtained at different facilities are comparable, with the average difference between quarters within the same set being $\sim$250%. Results of TDS in figure 4 are superimposed with the results of IBA scans of the corresponding tiles, demonstrating that the overall distribution of D across the tile is similar as measured by both techniques, with higher D retention in the wings (deposition-dominated zone) and lower in the center (which is dominated by erosion). The overall tendency is for TDS to show somewhat higher values of retention compared with IBA; this is particularly pronounced in the central region of a tile.

Figure 5 presents an example of a comparison of the spectra produced at different TDS facilities; normalized spectra are shown here to emphasize the shapes of the peaks. It is evident that all instruments capture the same fundamental shape of the spectrum, featuring a single well-defined release peak (it should be noted that shapes of the spectra of the samples originating from different parts of the original tile are different; some sets of quarters feature multiple release peaks). However, while the exact positions of release maxima obtained at Facilities A and D are essentially identical, the position of the peak of spectrum B is shifted towards a higher temperature by $\sim$40 K. Similar behavior is observed in all investigated sets of quarter samples. This shift in peak position is not a universal constant—for different sets of quarters it varies and generally lies in the range of $\sim$0–150 K. Moreover, it can be seen that it is not a constant offset—temperature shift increases with increase in the nominal temperature (presented by the arrows in the example in figure 5). The reason for this discrepancy will be explored in section 4.3.

Several selected samples underwent IBA measurements before and after TDS measurements were performed on them. Figure 6 presents the amount of D remaining in samples as a fraction relative to the initial amount measured prior to TDS

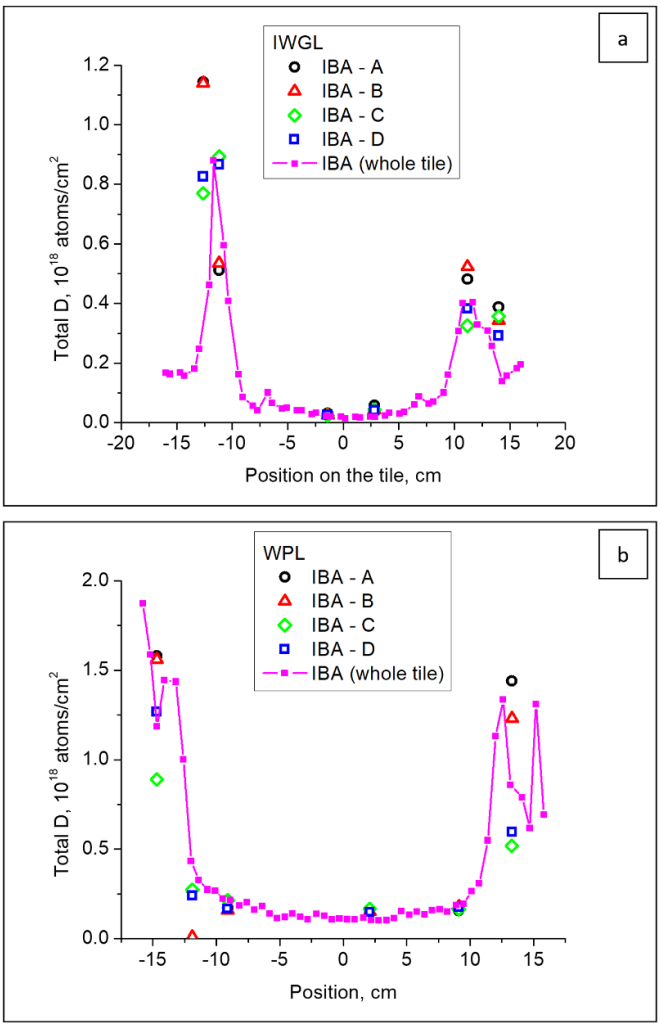

Figure 3. Comparison of the IBA results from quarter samples and corresponding IBA line scans: (*a*) IWGL tile and (*b*) WPL tile.

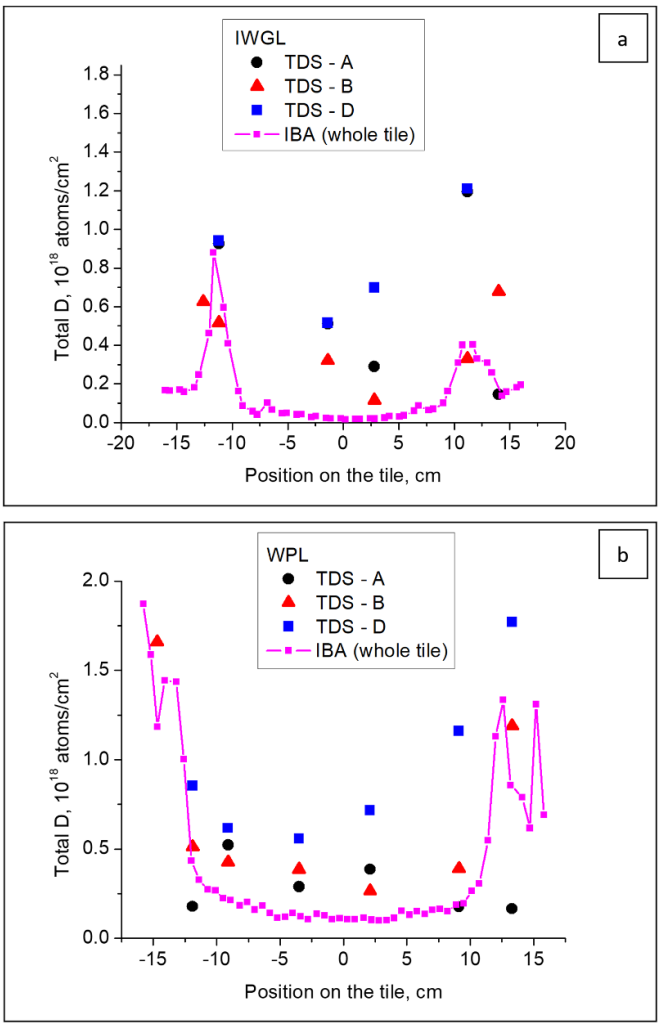

Figure 4. Comparison of the TDS results from quarter samples and corresponding IBA line scans: (*a*) IWGL tile and (*b*) WPL tile.

(as a percentage). It is evident that after a regular TDS run to a maximum temperature of 1050 K, a measurable fraction of D remains unreleased, up to ∼30% in some cases. As two of the TDS facilities, A and D, are capable of a maximum temperature of 1275 K, two sets of quarters were selected (specifically castellations 460 and 524), where the maximum temperature was different for the different samples: one sample was heated to 1050 K in Facility B and two to 1275 K in Facilities A and D. Figure 6 presents a comparison between the results, and it can be seen that heating to 1275 K significantly reduces the remaining fraction, by a factor of 5–15, bringing the unreleased fraction of D to less than 3%.

Figure 7 presents a comparison of the T content obtained from across the IWGL tile at TDS Facilities B and D and dissolution at Facility C. The difference between the TDS instruments is significant—close to two orders of magnitude in certain locations. At the same time, dissolution results are considerably lower than those of both TDS facilities, by up to almost three orders of magnitude.

3.2. *Reference samples*

The composition of the surface region of the tungsten coatings of the reference samples, including impurity content, measured using the ToF-ERDA method at UU is presented in table 2.

Comparison of the values of D retention in the reference samples, measured by IBA and TDS, is presented in table 3. Overall, the IBA results differ within ∼20%; TDS results are identical within ∼40%. In addition, in Facility B two samples from the set were measured, and the results for these two samples were very similar (less than 5% difference).

Comparison of the spectra produced in the three TDS facilities (figure 8; normalized spectra are presented) shows a specific trend. While all the spectra have similar overall shapes, the spectra produced at Facilities A and D have essentially identical positions of the release peaks. At the same time, results for Facility B show a tendency to shift towards higher temperature, with the magnitude of this shift increasing with

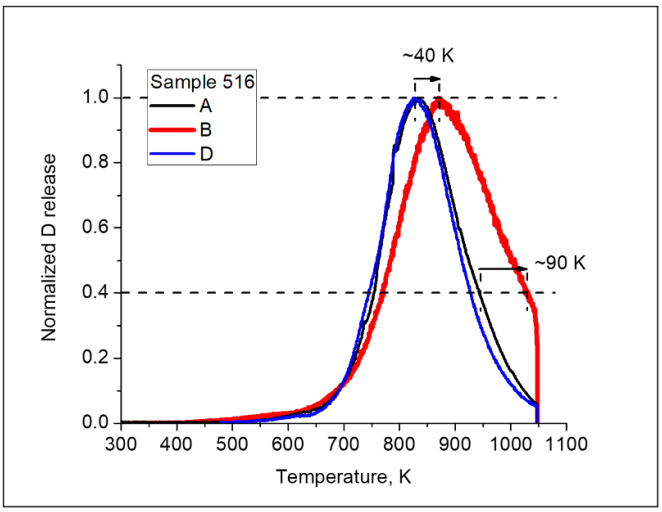

Figure 5. Comparison of the normalized D desorption spectra from a set of quarter samples measured at different facilities.

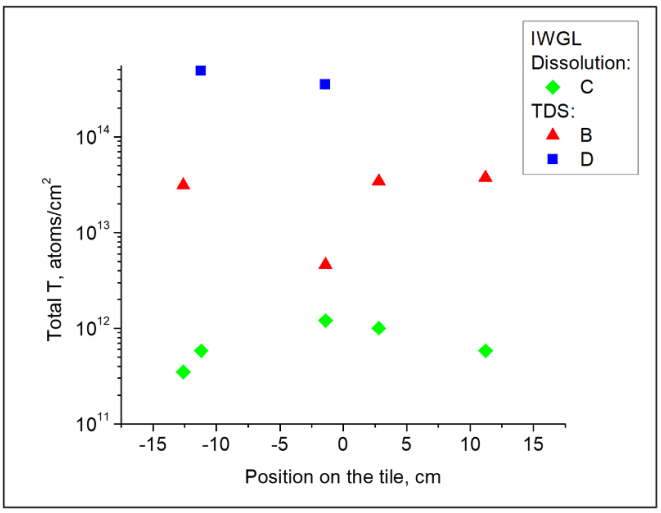

Figure 7. Comparison of amounts of T measured by TDS at different facilities and by dissolution.

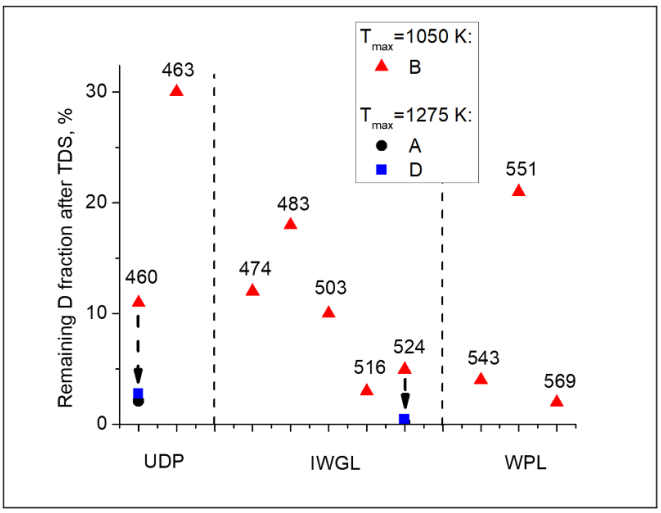

Figure 6. Remaining percentage of D measured by IBA after a TDS run relative to that measured by IBA before a TDS run, for specified samples.

temperature, similar to that observed in the quarter samples (section 3.1).

3.3. *Tritiated reference samples*

A comparison of the values of T retention in the tritiated samples, measured by TDS (at Facilities A and B; due to technical issues, measurements could not be performed at Facility D) and dissolution (Facility C), is presented in table 4. Overall the results vary by ∼220%. The difference between the results of dissolution and TDS at Facility B is within ∼36%. At the same time, the difference between dissolution and TDS at Facility A is larger, ∼140%.

Figure 9 presents a comparison between the normalized spectra of atomic T release measured at Facilities A and B. It is evident that the overall shapes of the spectra are similar, with peaks at ∼800 K and 1020 K, with the low-temperature peak being dominant. The positions of the peaks do not coincide exactly. The difference in the position of the low-temperature peak is ∼35 K (835 K for Facility A and 800 K for Facility B); the difference in the position of the high-temperature peak is ∼40 K (975 K for Facility B and 1015 K for Facility A).

Table 2. Composition of the surface region of the tungsten coatings in atomic concentrations (at.%) of elements.

Element	Concentration (at.%)
W	76.1
D	1.6
H	0.4
C	1.1
N	5.4
O	13.4
Ar	1.2

4. Discussion

4.1. *Measurements of deuterium retention*

From the perspective of the main topic of this work—determination of how comparable the results of different TDS facilities are—the main observation is that the results of TDS measurements on similar samples are quite comparable. The difference in measured values of total retention is ∼40% for highly reproducible reference samples. IBA was performed on each of the investigated samples as a way of independently verifying how similar they were in terms of D retention. IBA on two of the reference samples yielded values of 7.4×10^{17} and 8.8×10^{17} D cm^{-2} (a difference of ∼20%). This value can be considered a measure of the inherent difference between the reference samples due to manufacturing uncertainties, and hence the lower bound for the possible difference in D retention values measured by TDS. On the other hand, for these samples the results of TDS deviated by up to ∼40% between

Table 3. D retention (D cm^{-2}) in reference samples.

IBA IST	IBA UU	TDS, Facility A	TDS, Facility B (sample 1)	TDS, Facility B (sample 2)	TDS, Facility D
7.4×10^{17}	8.8×10^{17}	1.1×10^{18}	8.2×10^{17}	7.9×10^{17}	8.8×10^{17}

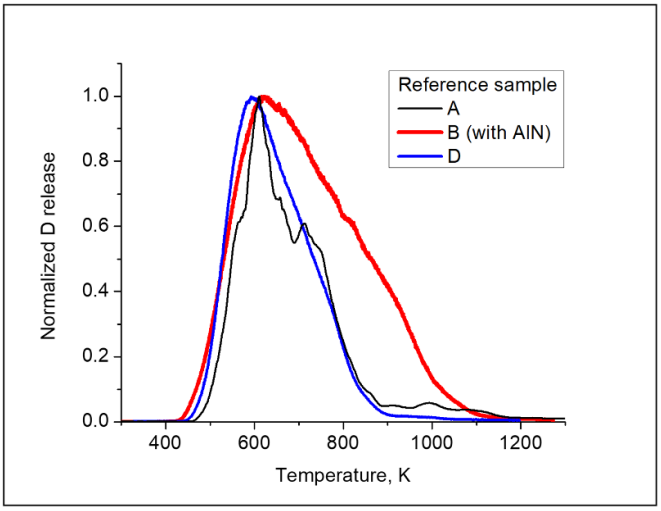

Figure 8. Comparison of the D desorption spectra obtained from reference samples at different facilities.

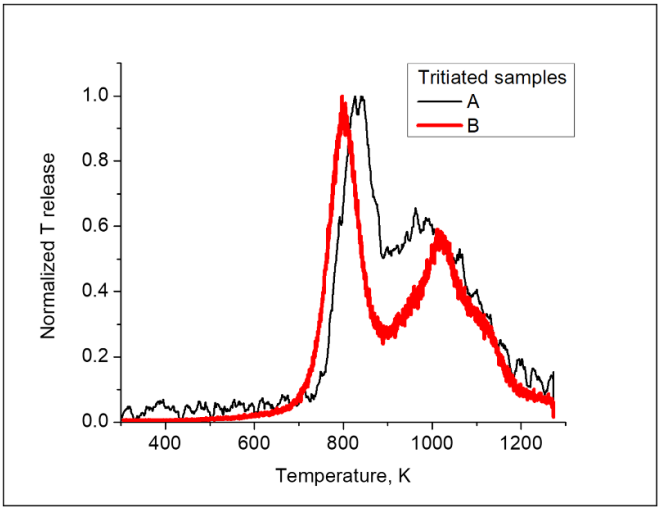

Figure 9. Comparison of the T desorption spectra obtained from reference samples at Facilities A and B.

Table 4. T retention in tritiated samples.

TDS, Facility A	TDS, Facility B	Dissolution, Facility C
5.75×10^{15}	1.85×10^{16}	1.36×10^{16}

the different facilities. The fact that the discrepancy in TDS results is larger than that for IBA results suggests that the observed difference includes a contribution from non-inherent discrepancies, i.e. pertaining specifically to TDS measurements. Notably, this TDS-specific discrepancy—the difference between total TDS and IBA discrepancies—is small, at only ∼20%. This is an encouraging result, indicating that, in general, similar samples do indeed yield similar results.

In the case of JET samples, the average difference between Be quarter samples within the same set is somewhat higher, at ∼250%. On the other hand, the average difference between the results of IBA within a set of quarters was ∼150%, which indicates that for these samples the TDS-specific discrepancy is larger (∼100%).

The TDS-specific discrepancies (which determine both the difference between measurements at different facilities and between TDS and IBA) are attributed to the following sources:

Factor 1: incomplete desorption leading to uncertainty in D quantification;

Factor 2: inherent difference between IBA and TDS techniques due to different sampling depths/volumes and sensitivity to inhomogeneities from quarter samples;

Factor 3: uncertainty of the QMS calibration;

Factor 4: unquantified fraction of D released in HDO and D_2O molecules.

In the following discussion these factors will be analyzed and referred to using the designation from this list.

Factor 1: from figure 6 it is evident that not all D is released from the Be quarter samples during a regular TDS run to the maximum temperature of 1050 K (and even when the maximum temperature is 1275 K, though to a much lesser extent), therefore it can be concluded that TDS measurements on Be samples will underestimate the true amount of D present (leading to Factor 1). However, this underestimation is relatively minor—the fraction of D that is undetected in TDS is ∼30% even in the worst cases, and is usually less than 20%. It should be noted that there is a significant scatter between the remaining fractions from sample to sample—the remaining D fraction ranges between ∼2% and 30% (figure 6). Comparison of the release spectra from the corresponding samples (figure 10) demonstrates that this difference in remaining D fraction originates from the difference in the position of the release maximum in the corresponding desorption spectrum. Samples with a large remaining fraction (such as 463B in the example in figure 10) are those where the release maximum is at higher temperature (in the case of 463B at 970 K), close to the maximum temperature of the TDS run (1050 K). As a consequence, at the beginning of the holding period the release rate is still high (comparable to that at the maximum), and hence by the end of the holding period, during which the release rate progressively decreases, the release rate is still substantial, reflecting a significant remaining amount of D. In

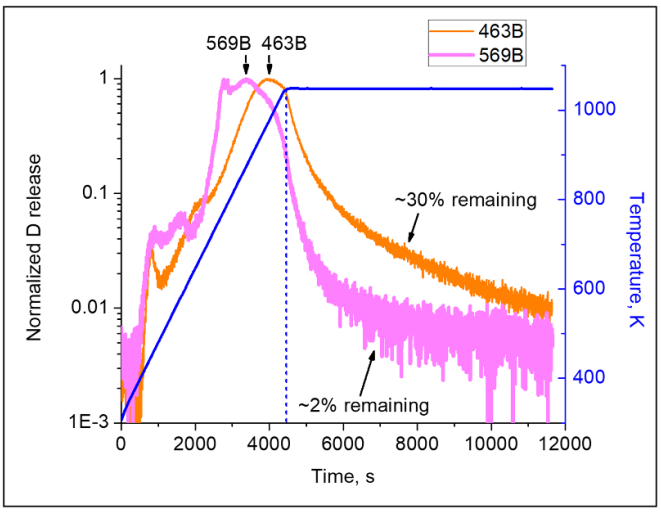

Figure 10. Comparison of the normalized D spectra obtained at Facility B using two samples with significantly different percentages of D remaining after a TDS run.

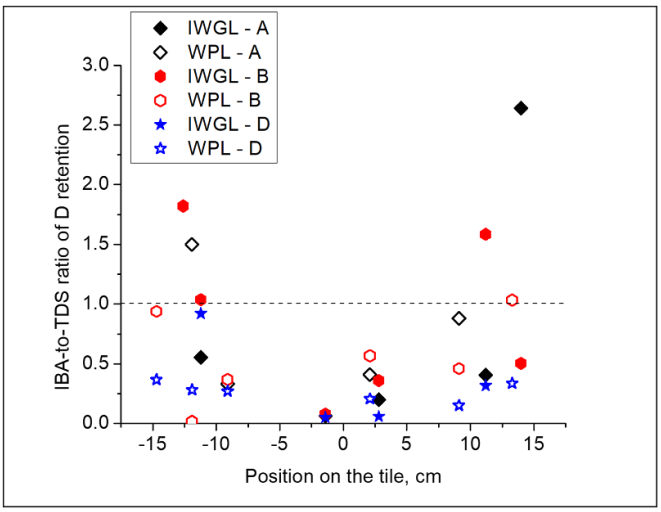

Figure 11. Comparison of the ratios of amounts of D measured by IBA and TDS for different quarter samples across IWGL and WPL tiles.

contrast, for those samples with the release maximum at lower temperatures (e.g. 569B in figure 10, at 880 K), the hold time is more effective at removing the remaining D, with the release rate falling to near-background levels by the end. Therefore, it can be expected that TDS results from Be samples where the release maximum is shifted to higher temperatures (in particular close to the maximum temperature of the run) will tend to have a higher degree of underestimation.

In light of this, it can be suggested that a preferable procedure for TDS measurements on Be samples is heating them up to the highest temperature available for the equipment, which in this case is a maximum temperature of 1275 K for Facilities A and D. However, when this is not possible, the degree of underestimation is of the order of a few tens per cent.

Factor 2: the ratio of D retention values measured by IBA to those of TDS for the same individual quarters is plotted as a function of position within a tile in figure 11, where the results from all facilities are summarized. Comparison between TDS and IBA results demonstrates that TDS tends to systematically yield higher values of D retention than IBA. This can be attributed to the fact that detection ranges (i.e. the depth to which retained D is detected) are different, with IBA only probing the near-surface region ($\sim$5 μm in the conditions implemented in this study) while TDS detects D coming from the entire sample volume, including the bulk region beyond the IBA detection range. Therefore, when comparing TDS and IBA an additional source of discrepancy due to this difference in probed ranges (Factor 2 in the list above) arises.

It is also evident that there is a certain spatial distribution of the difference between IBA and TDS. In the center of a tile, the IBA-to-TDS ratio of D retention is low and tends to increase towards the periphery. This indicates that in the center—which is an erosion-dominated zone—the majority of D is retained in the bulk, outside the first 5 μm from the surface, and is therefore governed by diffusion and trapping. At the same time, at the periphery—a deposition-dominated zone—the majority of trapping occurs within the co-deposits and the majority of the D is therefore located close to the surface, accessible to IBA probing.

It should be noted that it is unphysical to have a higher total retention measured by IBA than TDS, since by definition IBA only measures a fraction of the volume measured by TDS, thus the IBA-to-TDS ratio should never exceed 1. It can be seen, however, that in some cases, all of which are located at the periphery of the tiles (within the deposition-dominated zone), this ratio is higher than 1. This reflects the fact that the size of the ion beam spot is $\sim$1 mm^2, i.e. it is smaller than the dimensions of a quarter sample. Therefore, IBA results here are more sensitive to the local inhomogeneity of D content (such as individual D-rich co-deposit particulates, for example, which can be present within the beam spot leading to an increase in observed D content but not reflecting the true overall D content within the sample). Incidentally, this local inhomogeneity is a contribution to the observed variation in IBA results themselves noted in figure 3. Additionally, Factor 1 (incomplete D release) also contributes to the IBA-to-TDS ratio exceeding 1 as an underestimation of the total retention drives the IBA-to-TDS ratio up.

Factors 3 and 4: uncertainty in calibration and in the unaccounted for contribution of other D-containing molecules can be addressed by using the results from the reference samples, which, since they are lab-produced, are inherently more comparable. Importantly, Factors 1 and 2 from the list above are not relevant for the reference samples. W-coated Mo samples were heated to 1275 K and, as is evident from figure 8, D release ceased by the time the maximum temperature was reached, which means that no unreleased D remained unaccounted for in the sample following the TDS measurement. Hence one expects no discrepancy due to Factor 1. Since the D-saturated W layer is $\sim$2 μm thick, the IBA probing depth covers its

entirety, and thus the probed depth region is the same for IBA and TDS, eliminating the influence of Factor 2 as well.

It was noted above that the TDS-specific difference in D quantification between reference samples is ∼20%. Given the arguments above, this can be considered as an estimate of the combined contributions of Factors 3 and 4 to the discrepancy arising between TDS instruments. Deconvolution of these factors is not possible due to the difficulty in calibrating HDO and D_2O contributions, but these are very likely to be different between the systems. This conclusion stems from the fact that the relative contribution of HD and D_2 molecules is different between the instruments (the percentage of D released in the form of HD molecules is ∼17% in Facility B and ∼19% in Facility D, but ∼30% in Facility A), possibly due to different background levels of residual H_2 and in particular H_2O in the vacuum chambers; it is therefore reasonable to assume the kinetics of formation of other molecular species are also different. However, since the results of TDS instruments are generally similar in total D quantification and desorption characteristics, and also similar to IBA results, it can be concluded that contributions of unquantified D-containing molecular species (Factor 4) are small; correspondingly, the contribution of Factor 3 must be small as well.

Based on these findings it can be concluded that, barring severe experimental errors such as incorrectly determined calibration factors, values of retention reported from different laboratories are comparable for practical purposes. In particular, for highly reproducible lab-produced samples the discrepancy between the systems is only ∼20%. Technical solutions such as improved determination of calibration factors for D-containing molecules and improvement of vacuum in the measurement chamber (with the associated decrease of H_2 and H_2O backgrounds) can be recommended to improve the degree of measurement precision, and therefore comparability.

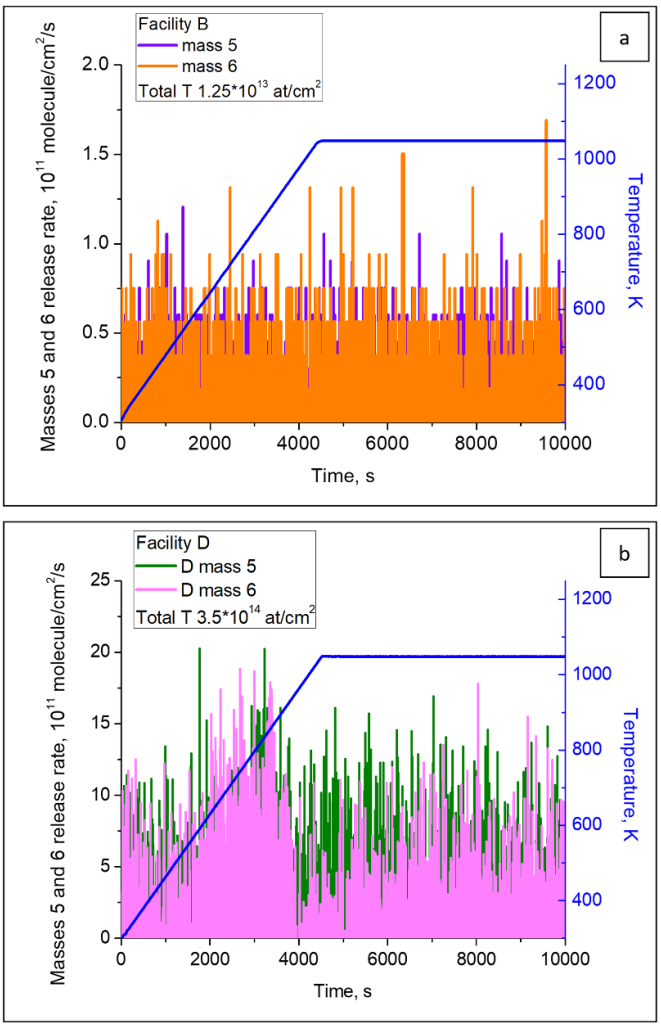

Figure 12. Typical desorption spectra of masses 5 and 6, measured at (*a*) Facility B and (*b*) Facility D.

4.2. Measurements of tritium retention

The data plotted in figure 7 show a large discrepancy (close to three orders of magnitude for some sets) in the T quantification of the quarter samples, both between different TDS instruments and between TDS and dissolution. However, on examining the mass 5 (DT) and 6 (T_2) spectra it is evident that these signals are essentially at the level of noise (see figure 12) and therefore T quantification using QMS signals of DT and T_2 molecules at these low concentrations is not possible. The intrinsic noise level will be governed by pumping and vacuum conditions for individual systems.

This could be expected, since at present only trace amounts of T are present in JET-ILW tiles. This is due to the fact that between the installation of ILW and extraction of the tiles used for the measurements following the ILW3 campaign, only H and D were used in JET, and thus all the T present comes either from implantation of energetic T produced in the D–D reaction or neutron-induced transmutation of Be, in addition to residual inventory from the previous D–T campaign in 1997 (pre-ILW) [92].

On the other hand, T contents obtained in dissolution measurements do not result from QMS-based detection of molecular species but derive from the direct measurements of radioactivity of released T. This activity can be accurately measured even at very low T concentrations, and these measurements are not affected by the molecular state of T. Therefore, it can be concluded that at the current T levels in Be tiles of JET-ILW—namely, on the order of 10^{12} atoms cm^{-2}—measurements of QMS-based TDS do not allow reliable quantification of T content and distribution. In contrast to these, the radiometry-based dissolution method, where activity of released T is measured, as opposed to detection of molecules by QMS, is much more sensitive to low concentrations of T and is therefore preferable for analysis of T distribution in JET tiles at the present T concentrations.

Lab-produced tritiated samples contained considerably higher amounts of T (∼10^{16} atoms cm^{-2}). Indeed, it can be seen that at this T content the results of TDS and dissolution are comparable (table 4), indicating that determination of T

content in QMS-based instruments becomes feasible when it is sufficiently high. The exact T content where this transition occurs has not been established. However, considering both the results from quarter samples and tritiated samples, an estimate can be suggested. As per figure 12, for QMS-based TDS the signals of T-containing molecules are at or close to the noise level; these correspond to the calculated T contents of 10^{12}–10^{14} atoms cm^{-2}, even when radiometrically measured contents are much lower. This suggests that any concentration of T below these levels would be lost in noise and is therefore not measurable by QMS-based TDS. Thus, the transition to a content where this measurement becomes possible with this technique lies in the range 10^{14}–10^{16} atoms cm^{-2}.

Despite the low concentration of T in the quarter samples presented here, it is important to note that in the 2021 DTE2 campaign in JET a 50%–50% D-T mixture was used, indicating that following this campaign the amount of T retained in the PFC will be comparable to that of D. Consequently, based on the results of tritiated reference samples, where the amount of T is comparable to that of D in typical JET samples and is reasonably confidently quantified using QMS-based TDS measurements, it can be expected that when PFCs are extracted from JET in the future (i.e. following the DTE2 campaign), quantitative studies of T retention using TDS will be possible. Of course, the same holds true for eventual studies of PFCs extracted from ITER.

4.3. Desorption spectra

Comparison of the desorption release spectra produced at different facilities demonstrates that overall shapes of the spectra are captured by all of them. However, a systematic difference was observed in terms of the positions of the release peaks. While Facilities A and D produce spectra with peaks at essentially identical temperatures, spectra from Facility B are systematically shifted towards a higher temperature. Moreover, as noted in sections 3.1 and 3.2, this shift is not a constant offset—the higher the temperature, the larger the shift.

To explain this behavior one should note that, as mentioned in the experimental description, Facilities A and D are using the same type of heating system, while the heating system of Facility B is different. In Facilities A and D, a sample is placed inside a quartz tube and heated within an oven; in contrast, in Facility B the sample is placed onto a heating plate with a protective AlN layer between the heater and the sample. It should be emphasized that the protective layer is necessary for use with Be samples to avoid bonding the sample to the stage as a result of localized heating, and while for W-coated Mo reference samples this is technically not necessary it was still done to keep the experimental conditions the same for comparison purposes. Therefore, it can be suggested that the difference in the way heating is applied lead to the observed changes in release temperatures.

The fact that there is no need to use an AlN layer with the reference W-coated Mo samples was utilized to study the effect of AlN on the spectral shapes and peak positions in Facility B. Two reference samples were measured, one with and one without an AlN layer. A comparison of the corresponding spectra is shown in figure 13, and it is evident that the presence of an AlN layer indeed modifies the spectrum in the same way as observed above—the positions of peaks shift towards higher temperature, and this shift increases with temperature. On the other hand, from figure 13 it is also evident that the peak positions produced without AlN in Facility B are close to those produced in Facility D, i.e. in the absence of AlN the above-mentioned systematic temperature discrepancy disappears.

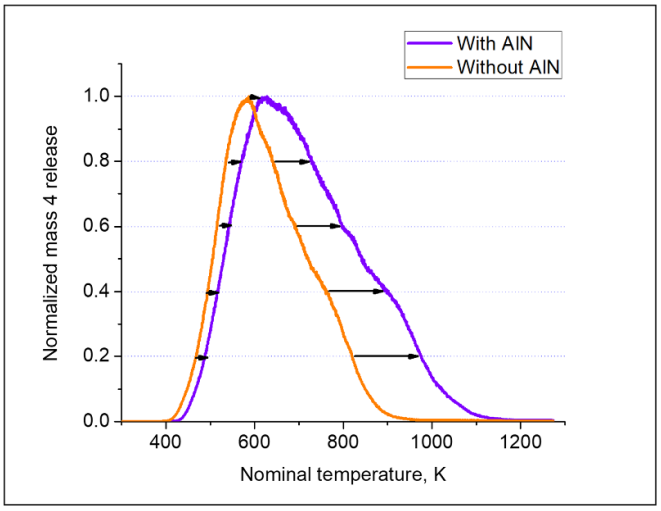

Figure 13. TDS spectra obtained for reference samples at different facilities, and in Facility B without a protective AlN layer.

This behavior can be explained as follows. Because of the additional step of thermal transfer through the AlN layer, as well as through the AlN–heater interface, the true temperature of the sample surface is lower than the nominal temperature measured at the heater, and this temperature delay between the heater and the sample increases with increase in the heater temperature. In the spectra produced at Facility B, the sample temperature (not measured directly) is considered to be equal to the heater temperature (which is the one that is measured and recorded). However, because of this delay, this assumption does not hold in the presence of the AlN layer, and the true temperature of the sample is lower than assumed.

Comparing the positions of the characteristic points in the spectra measured with and without AlN (in the case of the reference samples), as well as spectra of the quarter samples measured with AlN on the plate heater in Facility B and those without it in the oven in Facilities A and D, it is possible to quantify the effect of the heating delay due to the AlN layer. Figure 14(*a*) presents an example of such a procedure for a single spectrum. Arrows indicate the temperature difference created by the AlN layer at different nominal heater temperatures. Note that this assumes that such normalized spectra should be identical in the absence of AlN. The dependence of the temperature difference, calculated in such a way, on the

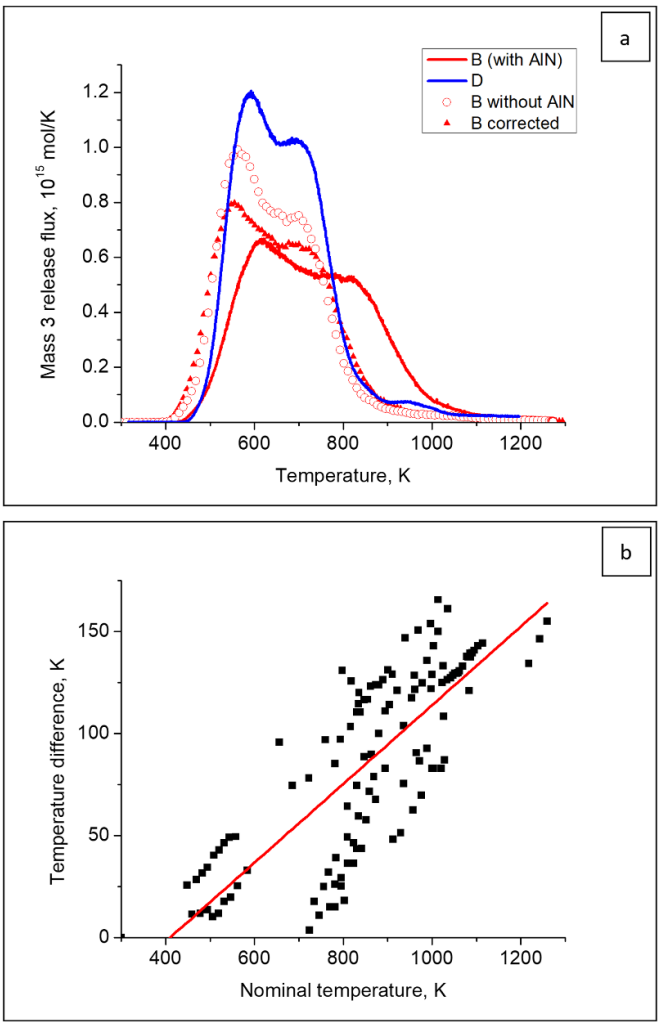

Figure 14. (*a*) Comparison of the normalized mass 4 release spectra obtained from the reference samples at Facility B with and without an AlN protective layer, illustrating the temperature shift introduced by AlN. (*b*) Dependence of temperature shift introduced by AlN on the nominal heater temperature.

nominal heater temperature is presented in figure 14(*b*). The points in the plot are taken from a number of spectra, comparing results for both W samples with and without AlN measured at Facility B and Be samples measured with AlN at Facility B with those measured at other facilities. It is evident that the increased temperature difference as a function of nominal temperature can be well fitted by a linear dependence with a slope of 0.193. This means that the temperature ramp experienced by the sample is still constant but it is lower than the nominal value of 10 K min^{-1}: it is equal to 10 × (1–0.193) = 10 × 0.807 or ∼8.1 K min^{-1}.

The heating rate at the sample surface can be used to perform a recalibration of temperature measurement and compensate, at least partially, the effect of the temperature delay introduced by the AlN layer. Since the heating rate is still constant, dependence of the sample temperature as a function of time can be calculated, replacing the heating rate at the heater stage, 10 K min^{-1}, by the calculated rate of 8.1 K min^{-1}. An example of a corrected spectrum produced in this way is shown in figure 13, and it is evident that the positions of the peaks in the corrected spectrum are similar to both those produced by the sample measured without AlN and those produced by the sample measured at a different facility.

It should be noted that, as seen in figure 14(*b*), there is a significant scatter of the values of temperature difference obtained from different samples—the deviation from the calibration line reaches ∼60 K. This can be considered to be an inherent uncertainty in the determination of sample temperature that cannot be eliminated by a single calibration function. Several factors contribute to this scatter in true surface temperature from sample to sample. Since D is mainly retained in the near-surface region, and the sample is heated from the opposite side on the plate heater, a certain temperature difference is introduced due to thermal transport within the thickness of the sample itself. This difference would depend on the material, and hence be different for W, bulk Be and Be co-deposits (where an additional thermal transport step through the deposit–substrate interface will be present), and indeed any other investigated material, but also on the thickness of the individual sample. In addition, sample-specific uncertainty arises also because different samples would have different shapes and roughness of the back surface, and as a result thermal contact between the surface and the sample will be different for each sample and cannot be quantified in a general way. Therefore, the influence of these different factors will vary from sample to sample but the figure of ∼60 K is a reasonable general estimate of the maximum uncertainty.

Since temperature positions of release peaks are used in the modeling of diffusion and trapping in order to determine trapping energies E_T for hydrogen isotopes in materials, the shift in temperature as measured by TDS can potentially influence the obtained values of E_T. In order to estimate to what degree the observed temperature uncertainty translates into the uncertainty in E_T, a simple analysis using the Kissinger method can be applied [93]. In this method, positions of the release peaks are measured at different heating rates and plotted as values of $\ln\left(\varphi/T_c^2\right)$ as a function of $1/T_c$, where φ is heating rate and T_c is peak temperature position, known as the Choo–Lee plot [94]. The trapping energy E_T is then related to the slope of the linear dependence of $\ln\left(\varphi/T_c^2\right)$ as $\frac{\partial\left(\varphi/T_c^2\right)}{\partial\left(1/T_c^2\right)} = -\frac{E_T}{R}$, where R is the gas constant.

Assume, as an example, a release peak located at 800 K with a heating rate of 10 K min^{-1}, corresponding to a trapping energy of 1 eV. Based on the assumed value of E_T the slope of the straight line can be calculated; from there, the intersections of this straight line with the lines corresponding to other heating rates can also be calculated, and hence the positions of release peaks that correspond to those heating rates can be determined—in this example, the peak would be located at 768 K at a heating rate of 5 K s^{-1} and 835 K at a heating rate of 20 K s^{-1} (circles in figure 15(*a*)). Now each of these peaks is shifted by an assumed value of temperature uncertainty, and correspondingly a new set of points in the Choo–Lee plot is formed (triangles in figure 15(*a*)). A straight line is then fitted to this newly formed set of points, its slope is calculated and

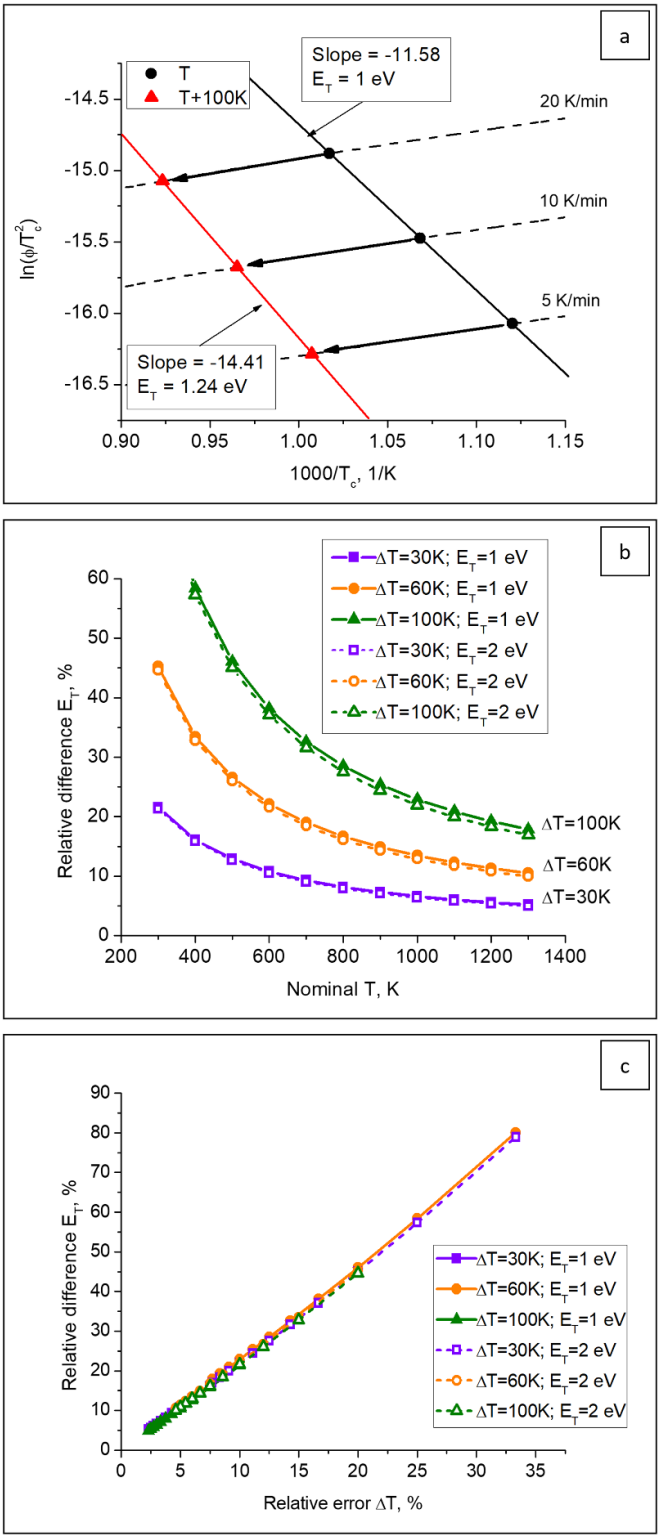

Figure 15. (*a*) An example of the simulated shift of peak positions caused by the temperature uncertainty of 100 K for heating rates of 5, 10 and 20 K min^{-1}. (*b*) Dependence of the relative uncertainty of E_T corresponding to the temperature uncertainties of 30, 60 and 100 K as a function of nominal temperature. (*c*) Dependence of the relative uncertainty of E_T as a function of relative temperature uncertainty.

a corresponding E_T is determined. In the particular example shown in figure 15(*a*), if a peak shifts by 100 K, the original value of 1 eV changes to 1.24 eV (a relative change of 24%).

Using this method, it is possible to calculate the relative uncertainty in E_T corresponding to an uncertainty in temperature measurement of 60 K. This is presented in figure 15(*b*) as a function of nominal heater temperature (for comparison, relative uncertainties caused by temperature uncertainties of 30 K and 100 K are also presented). Alternatively, the plots of relative uncertainty in E_T for different temperature uncertainties can be replotted as a function of relative temperature uncertainty, as presented in figure 15(*c*). It is evident that for any absolute temperature uncertainty such a dependence follows the same smooth curve. Notably, this relative change is almost independent of E_T, with a small decrease at higher trapping energies. It can be seen that in the temperature range where release peaks of Be samples are located, namely ∼800–1000 K, for a temperature uncertainty of 60 K (corresponding to a relative uncertainty of 6%–7.5%), the relative uncertainty in trapping energy is ∼15%.

In the context of the topic of this paper, the main conclusion with regard to the shapes of desorption spectra is that TDS facilities with different heating systems might produce spectra with somewhat different positions of the desorption peaks. Plate-type heaters, where samples are pressed to the flat heating surface and are heated from the back while desorption is detected from the front, tend to introduce random scatter in the positions of peaks, due to differences in sample geometry and mounting, and also introduce a systematic progressive shift of the spectra towards higher temperatures. However, this scatter, i.e. the temperature uncertainty, is shown to be in the range of several tens of kelvin, and this translates to a relatively small uncertainty in the determination of trapping energy (∼15% for the temperature range where desorption peaks are located in Be). Therefore, it can be concluded that quartz tube-type heating systems seem preferable as they are less susceptible to thermal gradients across the sample and associated uncertainty in sample temperature than the plate-type heating system for these types of samples that are relatively thick.

5. Summary and outlook

A comprehensive research exercise was designed and accomplished to address critical issues in quantification of the fuel inventory in Be- and T-contaminated PFCs from JET-ILW. In particular, the sources and the magnitudes of the discrepancies between the results obtained at independent TDS instruments as well as between TDS and other techniques, namely IBA (in the case of measurements of D content) and dissolution (in the case of T), were studied and quantified.

Insofar as measurements of D content in Be samples from JET are concerned, it was found that the discrepancy between different TDS instruments is close to ∼250%. Part of this discrepancy is due to the inherent differences between the

investigated samples, which were established to be ∼150% by IBA. The main sources of additional (TDS-specific), discrepancy (∼100%) include

(1) uncertainty of the remaining D content not released during the TDS measurement;
(2) uncertainty of the QMS calibration;
(3) unquantified fraction of D released in the form of HDO and D_2O molecules.

Uncertainty in the remaining content arises from the fact that in some TDS systems the maximum temperature to which a Be sample can be heated is limited by the onset of Be evaporation that starts above 1050 K. It was found that at this temperature up to ∼30% of D might remain unreleased, leading to a corresponding underestimation of measured retention. This underestimation is correlated with how close the maximum of the high-temperature release peak is to the beginning of the maximum temperature holding period, or, equivalently, what fraction of the maximum release flux is reached at the beginning of the hold. High remaining fractions are associated with a high release flux at the beginning of hold; when this release flux is down to ∼20% of the maximum, the remaining fraction of D is only several per cent. In contrast, heating to 1275 K, at which the temperature release flux is essentially nil, releases virtually all D present.

Combined uncertainties in the QMS calibration and the fraction of D released as unquantifiable molecular species (HDO and D_2O) are found to be small, generally ∼20% between different TDS laboratories.

Comparison of desorption spectra demonstrates that instruments with identical heating systems produce essentially identical spectra. It was found that a difference in the positions of desorption peaks could be observed between instruments with different heating systems (heating plate and oven). This difference has a characteristic appearance, where a system with a heating plate tends to produce spectra with release peaks at higher temperatures. This behavior can be explained by suppression of the heat transfer from the heater to the sample, leading to the actual temperature of a sample being lower than the assumed temperature (i.e. that of the heater). It has been demonstrated that a systematic temperature shift of this type can be partially corrected after the measurement. Following this correction, temperature uncertainty due to sample-specific variation is estimated to be ∼60 K. For Be, where release peaks are located in the 800–1000 K range, this translates into an uncertainty in the determination of trapping energy of ∼15%.

Comparison of TDS and IBA demonstrates that the ratio between amounts of D measured by two techniques at different locations across limiter tiles show a systematic dependence: in the central part of the tile the IBA-to-TDS ratio is low, generally below 0.5, and this increases towards the periphery, approaching 1. This indicates the difference in retention mechanism between these areas. In the erosion-dominated central part of a tile a large fraction of the D is retained in the bulk, beyond the detection range of IBA; on the other hand, in the deposition-dominated peripheral regions most of the retained D content is near the surface, within the reach of IBA. Indeed in the peripheral regions of the tiles, the IBA-to-TDS ratio occasionally exceeds 1, which is unphysical. This can be rationalized by the measurement spots of IBA occasionally containing local areas of increased D content, and does not reflect the amount of D in the sample as a whole, as well as underestimation by TDS of the total retention due to not all the D being released during a TDS run.

Comparison of T retention values indicate that at low T contents—corresponding to those found in JET-ILW PFCs at present, $\sim 10^{12}$–10^{14} atoms cm^{-2} (i.e. following only D plasma campaigns)—QMS-based TDS is not suitable for quantification, as opposed to radiometry-based methods such as dissolution. In contrast, at concentrations of $\sim 10^{16}$ atoms cm^{-2} QMS-based and radiometry-based techniques produce comparable results.

Based on the findings of the study, general recommendations regarding best practice for TDS measurements can be formulated:

(1) The maximum temperature in the TDS run should considerably exceed the temperature of the last release peak, such that by the beginning of the maximum temperature holding period the D release flux is considerably lower than at the maximum, ideally at most ∼20% of the maximum value. Otherwise, there is the potential for underestimating the values of retention.
(2) Accurate control and measurement of sample temperature is needed, making the oven-type heating systems preferable to heating plate-type ones, particularly for thick quarter samples.
(3) Systems should have the best vacuum that can be achieved to ensure the hydrogen and oxygen background is kept as low as possible, to minimize underestimation of the D content due to release of its fraction in the form of unquantifiable HDO and D_2O molecules and later T-containing iso-molecules.

Concerning comparison between different techniques, a few general observations can be made:

(1) TDS and IBA yield comparable results in terms of D retention. The differences in retention values that are observed in Be samples from JET-ILW limiter tiles are due to the different retention mechanisms in different regions of the tiles.
(2) TDS and dissolution yield comparable results in terms of T retention—with an important caveat that this is the case when T concentration is sufficiently high, above $\sim 10^{14}$–10^{16} atoms cm^{-2}. At lower T concentrations the T signal is below the limit of detection due to the intrinsic noise level, so QMS-based determination of T content is impossible. Radiometric techniques, such as dissolution of radiometry-based TDS, are preferable (indeed they present the only possibility) for measurements of T retention in these conditions (which, incidentally, characterize current T contents in JET-ILW PFCs).

Overall it should be emphasized that even though discrepancies were observed between different TDS facilities on the one hand and between TDS and other techniques on the other, these measurements can still provide valuable fuel quantification and trapping energy data. Even in the worst cases, discrepancy in retention of inhomogeneous samples and T between different TDS facilities is ∼250% (a factor of 3.5). For rather homogeneously prepared D and H reference samples a factor of 1.4 was determined between different TDS facilities. Comparison between different techniques shows that when their ranges of applicability overlap (i.e. comparing TDS and radiometry-based dissolution, when the amount of T is sufficiently high and comparing TDS and IBA when D is concentrated close to the surface within the probing range of IBA), their results are also comparable.

Acknowledgments

This work has been carried out within the framework of the EUROfusion Consortium, funded by the European Union via the Euratom Research and Training Programme (Grant Agreement No. 101052200—EUROfusion). Views and opinions expressed are, however, those of the author(s) only and do not necessarily reflect those of the European Union or the European Commission. Neither the European Union nor the European Commission can be held responsible for them.

This work has been part-funded by the EPSRC Energy Programme (Grant No. EP/W006839/1). To obtain further information on the data and models underlying this paper please contact PublicationsManager@ukaea.uk.

The research used UKAEA's Materials Research Facility, which has been funded by and is part of the UK's National Nuclear User Facility and Henry Royce Institute for Advanced Materials.

The work has been supported by the Swedish Research Council (VR), Grant 2015–04844. Financial support of the Tandem Accelerator Infrastructure by VR-RFI (contract #2017-00646_9) as well as the Swedish Foundation for Strategic Research (SSF) under contract RIF14-005 is gratefully acknowledged.

ORCID iDs

M. Zlobinski https://orcid.org/0000-0002-1395-7165
C. Porosnicu https://orcid.org/0000-0003-0561-0644
N. Catarino https://orcid.org/0000-0003-3879-1533
E. Pajuste https://orcid.org/0000-0003-1036-4679
L. Dittrich https://orcid.org/0000-0003-1933-8186
E. Alves https://orcid.org/0000-0003-0633-8937
G. Kizane https://orcid.org/0000-0002-3206-5322
M. Rubel https://orcid.org/0000-0001-9901-6296
A. Widdowson https://orcid.org/0000-0002-6805-8853

References

[1] Federici G. *et al* 2001 *Nucl. Fusion* **41** 1967
[2] Counsell G.C. *et al* 2006 *Plasma Phys. Control. Fusion* **48** B189
[3] Loarte A. *et al* 2007 *Nucl. Fusion* **47** S203 (ITER Physics Basis, Chapter 4)
[4] Rohde V., Maier H., Krieger K., Neu R. and Perchermaier J. 2001 *J. Nucl. Mater.* **290–293** 317
[5] Whyte D., Coad J.P., Franzen P. and Maier H. 1999 *Nucl. Fusion* **39** 1025
[6] Rubel M., Waelbroeck F., Bergsåker H., Wienhold P. and Emmoth B. 1989 *J. Nucl. Mater.* **161** 153
[7] Mayer M., Philipps V., Wienhold P., Esser H.G., von Seggern J. and Rubel M. 2001 *J. Nucl. Mater.* **290–293** 381
[8] Rubel M., Wienhold P. and Hildebrandt D. 2001 *J. Nucl. Mater.* **290–293** 473
[9] Skinner C.H. *et al* 1977 *J. Nucl. Mater.* **241–243** 214
[10] Mueller D. *et al* 1977 *J. Nucl. Mater.* **241–243** 897
[11] Coad J.P., Behrisch R., Bergsåker H., Ehrenberg J., Emmoth B., Partridge J., Saibene G., Sartori R., Simpson J.C.B. and Wen-Min W. 1989 *J. Nucl. Mater.* **162–164** 533
[12] Coad J.P. *et al* 1997 *J. Nucl. Mater.* **241–243** 408
[13] Coad J.P., Bekris N., Elder J.D., Erents S.K., Hole D.E., Lawson K.D., Matthews G.F., Penzhorn R.-D. and Stangeby P.C. 2001 *J. Nucl. Mater.* **290–293** 224
[14] Andrew P. *et al* 1999 *Fusion Eng. Des.* **47** 233
[15] Coad J.P., Rubel M., Likonen J., Bekris N., Brezinsek S., Matthews G.F., Mayer M. and Widdowson A.M. 2018 *Fusion Eng. Des.* **138** 78
[16] Penzhorn R.-D., Bekris N., Berndt U., Coad J.P., Ziegler H. and Nägele W. 2001 *J. Nucl. Mater.* **288** 170
[17] Rubel M., Coad J.P., Bekris N., Erents S.K., Hole D., Matthews G.F. and Penzhorn R.-D. 2003 *J. Nucl. Mater.* **313–316** 321
[18] Rubel M., Ivanova D., Philipps V., Zlobinski M., Huber A., Petersson P. and Schweer B. 2012 *Fusion Eng. Des.* **87** 935
[19] Matthews G.F. *et al* 2007 *Phys. Scr.* **T128** 137
[20] Matthews G.F. *et al* 2011 *Phys. Scr.* **T145** 014001
[21] Matthews G.F. 2013 *J. Nucl. Mater.* **438** S2
[22] Loarer T. *et al* 2013 *J. Nucl. Mater.* **438** S108
[23] Brezinsek S. *et al* 2013 *J. Nucl. Mater.* **438** S303
[24] Maas A.C. *et al* 1999 *Fusion Eng. Des.* **47** 247
[25] Hillis D.L., Klepper C.C., Von Hellermann M., Ehrenberg J., Finken K.H. and Mank G. 1997 *Fusion Eng. Des.* **34–35** 347
[26] Loarer T. *et al* 2007 *Nucl. Fusion* **47** 1112
[27] Tsitrone E. *et al* 2011 *J. Nucl. Mater.* **415** S735
[28] Pégourié B. *et al* 2013 *J. Nucl. Mater.* **438** S120
[29] Lässer R. *et al* 1999 *Fusion Eng. Des.* **47** 173
[30] Lässer R., Bell A.C., Grieveson B., Hemmerich J.L., Stagg R. and Atkins G.V. 1999 *Fusion Eng. Des.* **47** 333
[31] Summers D.D.D., Beurskens M.N.A., Coad J.P., Counsell G., Fundamenski W., Matthews G.F. and Stamp M.F. 2001 *J. Nucl. Mater.* **290–293** 496
[32] Huber A., Mayer M., Philipps V., Pospieszczyk A., Ohgo T., Rubel M., Schweer B., Sergienko G. and Tanabe T. 2001 *Phys. Scr.* **T94** 102
[33] Schweer B., Irrek F., Sergienko G., Philipps V. and Samm U. 2007 *J. Nucl. Mater.* **363–365** 1375
[34] Philipps V. *et al* 2013 *Nucl. Fusion* **53** 093002
[35] Malaquias A. *et al* 2013 *J. Nucl. Mater.* **438** S936
[36] Zlobinski M. *et al* 2020 *Phys. Scr.* **T171** 014075

[37] Hartwig Z.S., Barnard H.S., Sorbom B.N., Lanza R.C., Lipschultz B., Stahle P.W. and Whyte D.G. 2015 Fuel retention measurements in Alcator C-Mod using accelerator-based *in situ* materials surveillance *J. Nucl. Mater.* **463** 73

[38] Gierse N., Schweer B., Huber A., Karger O., Philipps V., Samm U. and Sergienko G. 2011 *J. Nucl. Mater.* **415** S1195–8

[39] Grisolia C. *et al* 2007 *In-situ* tokamak laser applications for detritiation and co-deposited layers studies *J. Nucl. Mater.* **363–365** 1138–47

[40] Semerok A., L'Hermite D., Weulersse J.M., Lacour J.L., Cheymol G., Kempenaars M., Bekris N. and Grisolia C. 2016 Laser induced breakdown spectroscopy application in Joint European Torus *Spectrochim. Acta* B **123** 121–8

[41] Widdowson A. *et al* 2007 *J. Nucl. Mater.* **363–365** 341

[42] Likonen J., Heinola K., De Backer A., Baron-Wiechec A., Catarino N., Jepu I., Ayres C.F., Coad P., Matthews G.F. and Widdowson A. 2019 *Nucl. Mater. Energy* **19** 300

[43] Baron-Wiechec A. *et al* 2015 *J. Nucl. Mater.* **463** 157

[44] Petersson P., Rubel M., Esser H.G., Likonen J., Koivuranta S. and Widdowson A. 2015 *J. Nucl. Mater.* **463** 814

[45] Heinola K. *et al* 2016 *Phys. Scr.* **T167** 014075

[46] Heinola K., Likonen J., Ahlgren T., Brezinsek S., De Temmerman G., Jepu I., Matthews G.F., Pitts R.A. and Widdowson A. 2017 *Nucl. Fusion* **57** 086024

[47] Heinola K. *et al* 2017 *Phys. Scr.* **T170** 014063

[48] Widdowson A. *et al* 2017 *Nucl. Mater. Energy* **12** 499

[49] Widdowson A. *et al* 2017 *Nucl. Fusion* **57** 086045

[50] Widdowson A. *et al* 2020 *Phys. Scr.* **T171** 014051

[51] Krat S. *et al* 2020 *Phys. Scr.* **T171** 014059

[52] Mayer M. *et al* 2016 *Phys. Scr.* **T167** 014051

[53] Rubel M. *et al* 2017 *Nucl. Fusion* **57** 066027

[54] Rubel M., Petersson P., Alves E., Brezinsek S., Coad J.P., Heinola K., Mayer M. and Widdowson A. 2016 *Nucl. Instrum. Methods* **B371** 4

[55] Mayer M. *et al* 2020 *Nucl. Fusion* **60** 025001

[56] Mayer M. *et al* 2009 *Nucl. Instrum. Methods* B **267** 506

[57] Bykov I., Petersson P., Bergsåker H., Hallén A. and Possnert G. 2012 *Nucl. Instrum. Methods* B **273** 250

[58] Kubota N. *et al* 2006 Surface analysis for TFTR armour tile exposed to D-T plasmas using nuclear technique *21th IAEA Conf on Fusion Energy* EX/P4-12 (available at: www-pub.iaea.org/MTCD/Meetings/FEC2006/ex_p4-12.pdf)

[59] Petersson P., Rubel M., Possnert G., Brezinsek S. and Pegourie B. 2012 *Nucl. Instrum. Methods* B **273** 113

[60] Ström P., Petersson P., Rubel M. and Possnert G. 2016 *Rev. Sci. Instrum.* **87** 103303

[61] Ström P., Petersson P., Rubel M., Fortuna-Zaleśna E., Widdowson A. and Sergienko G. 2019 *J. Nucl. Mater.* **516** 202

[62] Friedrich M., Pilz W., Sun G., Penzhorn R.-D., Bekris N., Behrisch R. and Garc?a-rosales C. 2001 *Phys. Scr.* **T94** 98

[63] Ruset C., Grigore E., Luculescu C., Tiseanu I., Likonen J., Mayer M., Rubel M. and Matthews G.F. 2016 *Phys. Scr.* **T167** 014049

[64] Likonen J., Lehto S., Coad J.P., Renvall T., Sajavaara T., Ahlgren T., Hole D.E., Matthews G.F. and Keinonen J. 2003 *Fusion Eng. Des.* **66–68** 219

[65] Zlobinski M. *et al* 2019 Laser-induced desorption of co-deposited deuterium in beryllium layers on tungsten *Nucl. Mater. Energy* **19** 503–9

[66] Xiao Q., Huber A., Sergienko G., Schweer B., Mertens P., Kubina A., Philipps V. and Ding H. 2013 *Fusion Eng. Des.* **88** 1813–7

[67] Oelmann J., Gierse N., Lia C., Brezinsek S., Zlobinski M., Turan B., Haas S. and Linsmeier C. 2018 *Spectrochim. Acta* B **144** 38–45

[68] Hatano Y., Widdowson A., Bekris N., Ayres C., Baron-Wiechec A., Likonen J., Koivuranta S., Ikonen J. and Yumizuru K. 2015 *J. Nucl. Mater.* **463** S966

[69] Hatano Y., Yumizuru K., Likonen J., Koivuranta S. and Ikonen J. 2016 *Phys. Scr.* **T167** 014009

[70] Lee S. *et al* 2020 *Fusion Eng. Des.* **160** 111959

[71] Lee S. *et al* 2021 *Nucl. Mater. Energy* **26** 100930

[72] Otsuka T. *et al* 2018 *Nucl. Mater. Energy* **17** 279

[73] Hatano Y. *et al* 2017 *Phys. Scr.* **T170** 014014

[74] Ashikawa N. *et al* 2020 *Nucl. Mater. Energy* **22** 100673

[75] Pajuste E., Kizane G., Vitins A., Igaune I., Avotina L. and Zarins R. (JET Contributors) 2017 Structure, tritium depth profile and desorption from 'plasma-facing' beryllium materials of ITER-Like-Wall at JET *Nucl. Mater. Energy* **12** 642–7

[76] Pajuste E. *et al* 2019 *Nucl. Fusion* **59** 106006

[77] Rubel M., De Temmerman G., Sergienko G., Sundelin P., Emmoth B. and Philipps V. 2007 *J. Nucl. Mater.* **363–365** 877

[78] Rebut H., Bickerton R.J. and Keen B.E. 1985 *Nucl. Fusion* **25** 1011

[79] Coad J.P., Bergsåker H., Burch S., Kaveney G., Lama F., Neill G.F., Partridge J., Simpson J.C.B. and Vince J. 1991 *J. Nucl. Mater.* **176–177** 145

[80] Petersson P., Rubel M., Possnert G. and Pegourie B. 2011 *Phys. Scr.* **T145** 014014

[81] Bykov I., Bergsåker H., Petersson P., Likonen J., Possnert G. and Widdowson A. 2015 *Nucl. Instrum. Methods* B **342** 19

[82] Gibney E. 2022 Nuclear-fusion reactor smashes energy record *Nature* **602** 371

[83] Catarino N., Barradas N.P., Corregidor V., Widdowson A., Baron-Wiechec A., Coad J.P., Heinola K., Rubel M. and Alves E. (JET conjtributors) 2017 *Nucl. Mater. Energy* **12** 559–63

[84] Matei L., Postolache C., Bubueanu G. and Podina C. 2008 Synthesis of labeled compounds using recovered tritium from expired beta light sources *Fusion Sci. Technol.* **54** 643

[85] Raty A., Lavonen T., Leskinen A., Likonen J., Postolache C., Fugaru V., Bubueanu G., Lungu C. and Bucsa A. 2019 Characterization measurements of fluental and graphite in FiR1 TRIGA research reactor decommissioning waste *Nucl. Eng. Des.* **353** 110198

[86] Fugaru V., Bubueanu G., Tuta C.S. and Ioan M.-R. 2020 Radiological characterization of the resulting solid materials from the refurbishment of the tritium laboratory *Fusion Sci. Technol.* **76** 347

[87] Dinca P., Staicu C., Porosnicu C., Pompilian O.G., Banici A.M., Butoi B., Lungu C. and Burducea I. 2021 *Coatings* **11** 1430

[88] Baron-Wiechec A., Heinola K., Likonen J., Alves E., Catarino N., Coad J.P., Corregidor V., Jepu I., Matthews G.F. and Widdowson A. 2018 Thermal desorption spectrometry of beryllium plasma facing tiles exposed in the JET tokamak *Fusion Eng. Des.* **133** 135–41

[89] Zlobinski M. *et al* 2019 *Fusion Eng. Des.* **146** 1176–80

[90] Catarino N., Widdowson A., Baron-Wiechec A., Coad J.P., Heinola K., Rubel M., Barradas N.P. and Alves E. (JET Contributors) 2020 *Phys. Scr.* **T171** 014044

[91] Pajuste E., Kizane G., Avotina L., Teimane A.S., Lescinskis A. and Vonda K. 2019 *Nucl. Fusion* **59** 10

[92] Pajuste E., Teimane A.S., Kizane G., Avotina L., Halitovs M., Lescinskis A., Vitins A., Kalnina P., Lagzdina E. and Zabolockis R.J. 2021 *Phys. Scr.* **96** 124050

[93] Kissinger H.E. 1957 Reaction kinetics in differential thermal analysis *Anal. Chem.* **29** 1702–6

[94] Choo W. and Lee J. 1982 Thermal analysis of trapped hydrogen in pure iron *Metall. Mater. Trans.* **13A** 135–40